RSC Advances

PAPER

View Article Online
View Journal | View Issue



Cite this: *RSC Adv.*, 2026, **16**, 12827

# Chemical and morphological evolution of hybrid conversion coatings in low-Earth orbit space environment

Ankita Mohanty, [a] Xiaoyang Liu,[ab] Cheng-Chu Chung, [a] Donald Vonk,[c] Kim Kisslinger, [d] Xiao Tong, [d] Stanislas Petrash,[e] Kathryn Foster[c] and Yu-chen Karen Chen-Wiegart *[af]

Understanding how protective coatings respond to the harsh low-Earth orbit (LEO) environment is essential for ensuring the safety, longevity, and cost-effectiveness of spacecraft. In particular, identifying environmentally friendly, non-chromate alternatives that can maintain performance under such conditions has both technological and regulatory significance. This study investigates the environmental stability of zirconium-based hybrid conversion coatings with Cu additives (Cu10 and Cu20) applied to cold-rolled steel, tested in the Materials International Space Station Experiment (MISSE) outside the International Space Station (ISS). Chemical and morphological analyses were carried out using a combination of electron microscopy and X-ray spectroscopy techniques, including scanning electron microscopy (SEM), scanning transmission electron microscopy with energy-dispersive X-ray spectroscopy (STEM-EDS), X-ray photoelectron spectroscopy (XPS), and X-ray absorption near-edge structure (XANES) spectroscopy. After exposure outside the ISS, all coatings remained structurally intact, with all exhibiting a uniform Zr-rich matrix and embedded Cu-rich clusters, while a thin Si-rich surface layer developed from interaction with space environments. Depth-resolved XPS showed a layered structure with CuO on the surface, $Cu_2O$, and partial Zr(IV) reduction near Cu-rich sites, evidence of Atomic Oxygen (AO)-driven surface oxidation. These results demonstrate that Cu–Zr coatings maintain their chemical integrity and microstructure in harsh space environments, offering a non-chromate alternative for long-term aerospace protection. These insights provide valuable guidance for developing next-generation protective coatings that combine environmental sustainability with the reliability required for future aerospace and orbital applications.

Received 19th December 2025
Accepted 23rd February 2026

DOI: 10.1039/d5ra09810f

rsc.li/rsc-advances



## 1. Introduction

Materials durability in low Earth orbit (LEO) is critical to the success and longevity of space missions, including operations aboard the International Space Station (ISS). In this environment, materials are exposed to a unique combination of stressors—atomic oxygen (AO), ultraviolet radiation, high vacuum, and repeated thermal cycling—that can lead to erosion, oxidation, mechanical fatigue, and coating failure. These effects pose significant risks to spacecraft reliability, service life, and maintenance costs.[1]

However, maintaining material performance in LEO is challenging due to the extreme and combined effects of AO bombardment, repeated thermal cycling, high vacuum, and radiation exposure. Materials on the ISS experience rapid temperature fluctuations during each 90 minute orbit,[2] inducing thermal fatigue and mechanical stress, while AO formed by photodissociation of molecular oxygen drives surface erosion. Ultra-high vacuum conditions promote outgassing and contamination, and exposure to ultraviolet radiation, plasma interactions, micrometeoroids, and orbital debris further accelerates degradation. Even AO-resistant coatings can fail locally due to thermal expansion mismatch and defect-driven erosion, enabling deeper AO penetration. Collectively, these factors lead to erosion, embrittlement, and structural weakening, underscoring the need for durable, long-lasting protective coatings for spacecraft materials operating in LEO.[2–4]

A solution to the above problems is the use of chemical conversion coatings that are widely applied as a surface

[a]*Department of Materials Science and Chemical Engineering, Stony Brook University, Stony Brook, NY 11794, USA. E-mail: Karen.Chen-Wiegart@stonybrook.edu*
[b]*X-ray Science Division, Argonne National Laboratory, Lemont, IL 60439, USA*
[c]*Henkel Corporation, Madison Heights, MI 48071, USA*
[d]*Center for Functional Nanomaterials, Brookhaven National Laboratory, Upton, NY 11973, USA*
[e]*Henkel Corporation, Bridgewater, NJ 08807, USA*
[f]*National Synchrotron Light Source II, Brookhaven National Laboratory, Upton, NY 11973, USA*

treatment to metallic substrates to combat erosion Traditionally, hexavalent chromium-based conversion coatings, often combined with fluorides or phosphates, have been the most common method for achieving these goals. These coatings provide excellent protection. Extensive research on the ISS, particularly through the MISSE (Materials International Space Station Experiment) missions, has been dedicated to evaluating the corrosion performance of traditional and alternative conversion coatings under true space conditions. In earlier MISSE missions such as MISSE-3 and MISSE-6B, chromate-based coatings (*e.g.*, Anadite and Iridite) applied on aluminum alloys like 2219-T851 and 2195 Al–Li were tested.[5] These coatings demonstrated excellent corrosion resistance and minimal optical degradation, retaining their barrier properties even after prolonged exposure to the harsh LEO environment. However, as regulatory pressures and environmental concerns around hexavalent chromium ($Cr^{6+}$) arose, the need for non-toxic, chromium-free alternatives has become increasingly urgent. Hexavalent chromate, while effective, is classified as a carcinogen and poses significant health and disposal challenges.[6] As a result, chrome-free coatings are being actively investigated for aerospace use to comply with evolving global regulations such as REACH and OSHA.[7,8] To address this, MISSE-7B included chrome-free conversion coatings such as Bonderite M-NT 5700 and Boegel, both applied to aluminum alloy substrates and exposed on the ISS for approximately 18 months. Post-flight analysis revealed minor physical and optical degradations, including slight discoloration and small changes in solar absorptance, but both coatings largely retained their corrosion protection.

Among the most promising chrome-free candidates are hexafluorozirconic acid ($H_2ZrF_6$)-based conversion coatings, which have demonstrated excellent corrosion resistance, chemical stability, and strong adhesion properties in terrestrial and laboratory studies across various metal substrates, including aluminum, magnesium, and steel.[9] These coatings are typically formed by immersing the metal substrate in chemical baths containing $H_2ZrF_6$.[10] The reaction between the solution and the metal substrate generates a protective Zr oxide-rich layer that shields the underlying metal from environmental degradation. Inorganic additives are commonly incorporated into hexafluorometallate-based coatings to modify the deposition behavior, increase surface roughness, and improve mechanical adhesion.[11] Specifically, the incorporation of $Cu^{2+}$ ions has been shown to enhance coating growth by promoting the formation of cathodic sites, accelerating the conversion reaction, and facilitating the deposition of fine Cu clusters on the surface.[12] Several studies have shown that incorporating $Cu^{2+}$ additives into the Zr-based coating bath can tune the microstructure of the coating, promote uniform film formation, and improve overall protective performance by accelerating cathodic site generation and forming nanoscale copper-rich clusters.[11,13–15] Studies have also examined the co-addition of $Cu^{2+}$ ions with polyamidoamine (PAMAM) dendrimers, demonstrating that appropriate PAMAM concentrations can prevent void formation and improve coating uniformity and adhesion.[14] This combination of Zr-based chemical conversion coatings modified with $Cu^{2+}$ additives represents a compelling, non-toxic alternative to traditional chromate systems.

Despite promising laboratory results, the long-term behavior of Zr–Cu hybrid conversion coatings under actual LEO conditions have not yet been evaluated in a MISSE mission. This lack of in-space validation limits their qualification for mission-critical aerospace applications.

In this work, we apply a Zr-based chemical conversion coating with $Cu^{2+}$ additives as a promising eco-friendly alternative to conventional chromate systems. To systematically investigate this coating system, we employed a multi-modal characterization approach, combining X-ray absorption spectroscopy (XAS), X-ray photoelectron spectroscopy (XPS), scanning electron microscopy (SEM), and transmission electron microscopy (TEM). By comparing samples exposed to the LEO environment at the ISS with corresponding Earth-stored controls as well as pristine coating samples, this study reveals how the harsh space environment affects the chemical integrity, microstructural evolution, and protective performance of Zr-based hybrid conversion coatings, while elucidating how different Cu loadings influence coating stability and redox response under space exposure. The analyses demonstrate their potential as sustainable, high-performance coatings for aerospace applications.

## 2. Methods

### 2.1 Substrate preparation

Low-carbon steel (LCS) sheets, specifically AISI 1008 cold-rolled steel (C $\leq$ 0.10 wt%, Mn 0.30–0.50 wt%, balance Fe), were used as the substrate. The 1008 cold-rolled steel (CRS) sheets were purchased from ACT Test Panels. The sheets, cut into dimensions of 5 mm by 5 mm, were initially sonicated in ethanol for 10 minutes to remove any surface impurities. This was followed by a deionized (DI) water rinse for one minute. The clean samples were dried using compressed air and then immersed in the coating solution as discussed below.

### 2.2 Preparation of chemical conversion coating solutions and their deposition on the substrate

The composition of the CC solutions involved mixing varying concentrations of $Cu^{2+}$ ions (10 and 20 ppm) with a fixed amount of PAMAM dendrimers (50 ppm). These mixtures are designated with identifiers such as Cu10 and Cu20, where the number corresponds to the concentration of $Cu^{2+}$ in parts per million used in the preparation of the coating. Details regarding these Zr-based CCs have been previously reported in the literature, as referenced in publication.[16] The conversion coating solution consists of hexafluorozirconic acid with the Cu added to the solution as cupric nitrate to maintain a zirconium content of 50–300 ppm while maintaining a consistent PAMAM level of 50 ppm. The pH level for all solutions was maintained at 4.0. The sample preparation details are shown in Fig. 1.

The initial step in the chemical CC process involved cleaning the substrate using an alkaline solution (pH $\sim$ 11.7), specifically Bonderite C-AK T51 (Henkel Corporation, Madison Heights, MI,

 

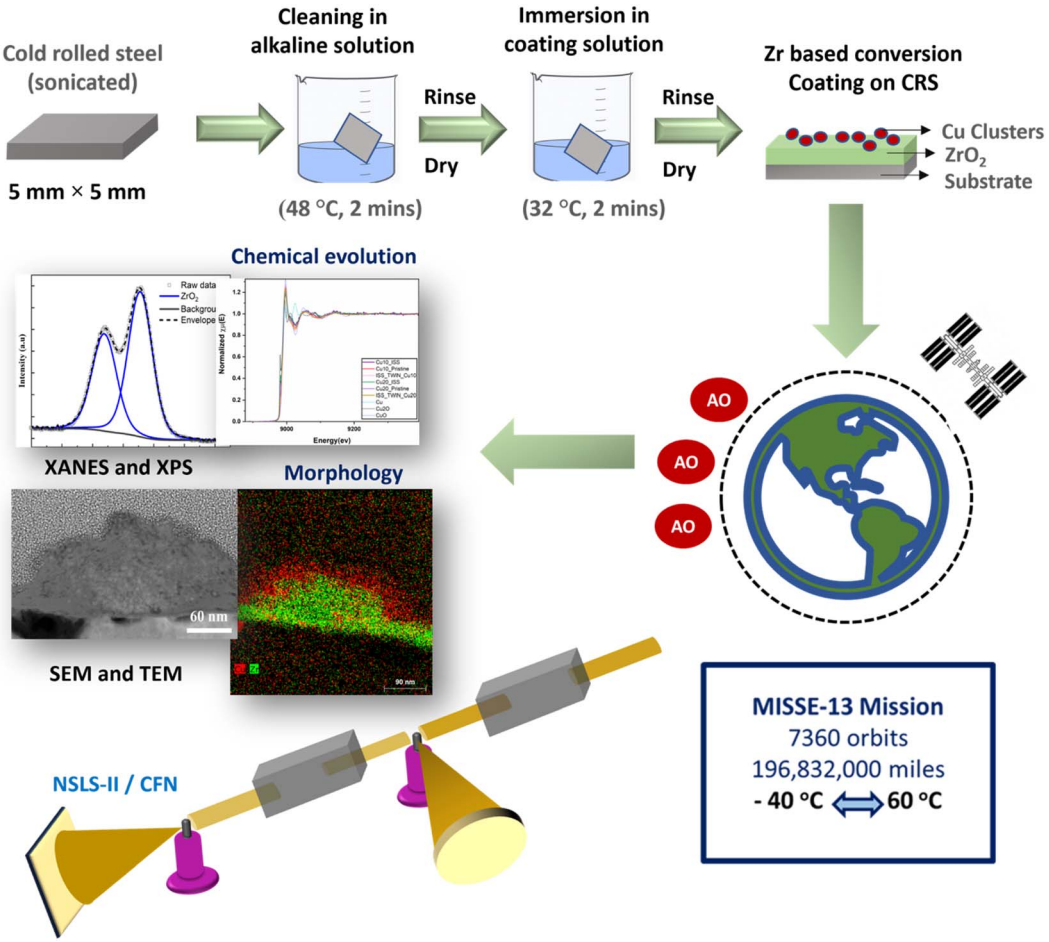


Fig. 1 Preparation of Zr-based conversion coating on CRS substrate, followed by exposure during the MISSE-13 mission outside the International Space Station. All schematic illustrations were created by the author. The samples returned to Earth were then subsequently analyzed using X-ray and electron-based characterization methods.

USA). This cleaning solution was comprised of potassium hydroxide (KOH), sodium hydroxide (NaOH), sodium nitrite ($NaNO_2$), and sodium silicate ($Na_2SiO_3$). The substrates were treated in this solution within a 150 ml glass beaker for 120 seconds at 48 °C, situated in a water bath, and subsequently rinsed with DI water for 60 seconds, followed by drying them with compressed air. Post-cleaning, the substrates were immersed in hybrid coating solutions for another 120 seconds at 32 °C to form the coating film. The coating solution, Bonderite M-NT 1820 (Henkel Corporation, Madison Heights, MI, USA), included hexafluorozirconic acid ($H_2ZrF_6$), polyamidoamine (PAMAM), and a Cu compound additive. The final step involved rinsing the samples in DI water for 60 seconds to remove any residual solution, followed by drying them with compressed air at room temperature.

### 2.3 Sample conditions and dispatch to the ISS

For the coating solutions Cu10 and Cu20, three distinct sample conditions were prepared: (1) the pristine samples, which represents the as-coated condition, characterized right after fresh preparation described in Section 2.2; (2) the ISS samples, which was subjected to the space environment on the ISS, with details described below; and (3) the twin samples, which was exposed to the Earth's atmosphere and was stored in the desiccator, for the same length of time as the ISS-exposed sample. The pristine and twin samples serve as references to isolate the effects of LEO exposure.

The ISS samples were prepared as follows: as-coated Cu10 and Cu20 samples were transported to the ISS on a payload managed by Alpha Space Test and Research Alliance, LLC. As part of the MISSE-13 mission, the samples orbited Earth approximately 7630 times from March 7, 2020, to July 10, 2021 (~500 days), covering a distance of nearly 196 832 000 miles from launch to splashdown. The samples were integrated into one standard 1 inch square mounting frame on a ram facing carrier of the MISSE flight facility. Throughout the mission, the samples experienced periodic thermal cycling ranging from −40 °C to +60 °C. Fig. S1 shows the certificate of the space flight as received by Stony Brook University for the successful completion of the mission. Following retrieval from the mission, the ISS samples were promptly transferred to an Ar-filled glovebox to preserve surface conditions before detailed characterization.

### 2.4 Surface characterization of the coating film

The surface morphology of the coating films was analyzed using a JEOL 7600F scanning electron microscope (SEM), operating at an accelerating voltage of 5.0 keV. A dual-beam FEI Helios scanning electron/focused ion beam microscope (FIB-SEM) was utilized for preparing cross-sectional images and extracting specimens for transmission electron microscopy (TEM) analysis by a lift-out method. Platinum (Pt) was first deposited as the protective layer prior to the lift-out procedure, followed by an established protocol, with final gallium ion ($Ga^+$) milling performed at 5 keV, extracted, and mounting the samples onto a TEM sample holder. The prepared specimens were then affixed to Omniprobe lift-out molybdenum (Mo) grids provided by Ted Pella, Inc. Subsequently, a high-resolution FEI Talos F200X scanning/transmission electron microscope (S/TEM), equipped with high-angle annular dark-field (HAADF) imaging and EDS capabilities, was employed to assess the elemental distribution within the coating, performed at an accelerating voltage of 200 keV. HAADF-STEM imaging was performed with a detector collection angle range of 28–170 mrad.

For chemical composition analysis, the coatings were examined using X-ray photoelectron spectroscopy (XPS) in an ultrahigh-vacuum (UHV) environment ($<2 \times 10^{-9}$ torr), utilizing a SPECS PHOIBOS 100 hemispherical electron energy analyzer and a SPECS XR50 Twin anode X-ray source with Al K$\alpha$ radiation (1486.6 eV). XPS data collection was done at the Center for Functional Nanomaterials (CFN) at Brookhaven National Laboratory (BNL). XPS data, including the C 1s peak at 284.8 eV, were processed with Shirley background subtraction, calibrated, and analyzed using CasaXPS software. To evaluate the oxidation states of Cu and Zr, high-resolution Cu 2p and Zr 3d spectra were collected and deconvoluted. The deconvoluted Cu $2p_{3/2}$ and Zr $3d_{5/2}$ spectra showed clear differences in oxidation states and surface composition across the different environments. The fitting parameters for Cu $2p_{3/2}$ in Cu10 and Cu20 are detailed in Table S1.

### 2.5 Characterization using X-ray absorption fine structure spectroscopy (XAFS)

X-ray Absorption Near-Edge Structure (XANES) spectroscopy was employed to study the chemical states and compositions of Zr and Cu in hybrid coatings, comparing samples maintained in Earth's atmosphere with those exposed to the space environment. This technique provided detailed insights into the elemental changes and interactions resulting from different environmental exposures. These measurements were conducted at the Beamline for Materials Measurement (BMM) located at the National Synchrotron Light Source II (NSLS-II) within Brookhaven National Laboratory. The experiments were conducted at the Zr K-edge ($\approx$17.998 keV, $\lambda \approx 0.689$ Å) and Cu K-edge ($\approx$8.979 keV, $\lambda \approx 1.381$ Å) using a grazing-incidence geometry to enhance surface sensitivity. The incident X-ray beam energy resolution ($\Delta E/E$) was on the order of $1.3 \times 10^{-4}$ as determined by the Si(111) double-crystal monochromator at the BMM The setup utilized a grazing-incidence approach to enhance the surface sensitivity of the samples. During data collection, the samples were rotated to minimize interference from Bragg diffraction signals emanating from the crystalline substrate. This diffraction contributes to a broad background that was later subtracted in the data analysis process.[17]

X-ray absorption spectra of Cu10 and Cu20 samples in three different conditions (pristine, ISS, and twin) were measured at the Zr and Cu K-edges to analyze the chemical states of the samples. Spectra for energy calibration and reference materials were acquired using standard materials including Zr, Cu foil, and powders of $ZrO_2$, CuO, and $Cu_2O$, all measured in transmission mode at the same beamline. The analysis of the XANES data was performed using the Athena software package. To enhance the signal-to-noise ratio of the data, averages were taken from six scans of the Zr and Cu K-edge energies from each sample. Post-collection, the absorption spectra underwent processing that included background subtraction and normalization.

## 3. Results and discussion

### 3.1 Influence of different environmental conditions on the surface morphology of the coating film

The surface morphologies of Cu10 and Cu20 coatings under different environmental conditions, pristine, ISS, and twin, are shown in Fig. 2A and B, respectively. In the pristine state, both coatings display well-distributed Cu clusters across the surface, with Cu20 exhibiting larger and more densely packed clusters than Cu10. This variation is attributed to the higher $Cu^{2+}$ concentration used in the Cu20 precursor solution, which promotes greater nucleation sites for Cu during deposition; this is consistent with the design of the coating and well-characterized in the previous studies.[10,12,14]

Following deployment on the MISSE platform outside the ISS, the coatings were exposed directly to the harsh conditions of LEO outside of the ISS, including intense AO bombardment, UV, high vacuum, and thermal cycling approximately every 90 minutes as the ISS orbited Earth. Without active thermal control, MISSE-mounted samples experienced extreme surface temperature swings, cooling to around −40 °C in orbital shadow and heating to about +60 °C in full sunlight.[18] Despite being exposed to these harsh conditions for over 1.5 years, both Cu10 and Cu20 samples retain their overall surface morphology, with Cu clusters still visible and coating integrity maintained. A closer inspection reveals a notable difference in how each system responded to the space environment. The Cu10 ISS sample shows some signs of slight disintegration, as indicated in red arrows in Fig. 2A with some cracks and a rougher surface. Here, disintegration refers specifically to these morphological changes, rather than direct chemical decomposition. This micro-cracks, partial fragmentation of surface features may be the result of lower overall Cu content in Cu10, which makes the surface more susceptible to AO attack, thermal cycling induced stress, or other factors. In contrast, the Cu20 ISS sample shows very subtle changes in comparison to Cu10. The higher Cu content may lead to the formation of more protective oxide ($Cu_2O$ or CuO) layers, serving as a passivation layer that could limit the AO interaction. While SEM reveals the

 

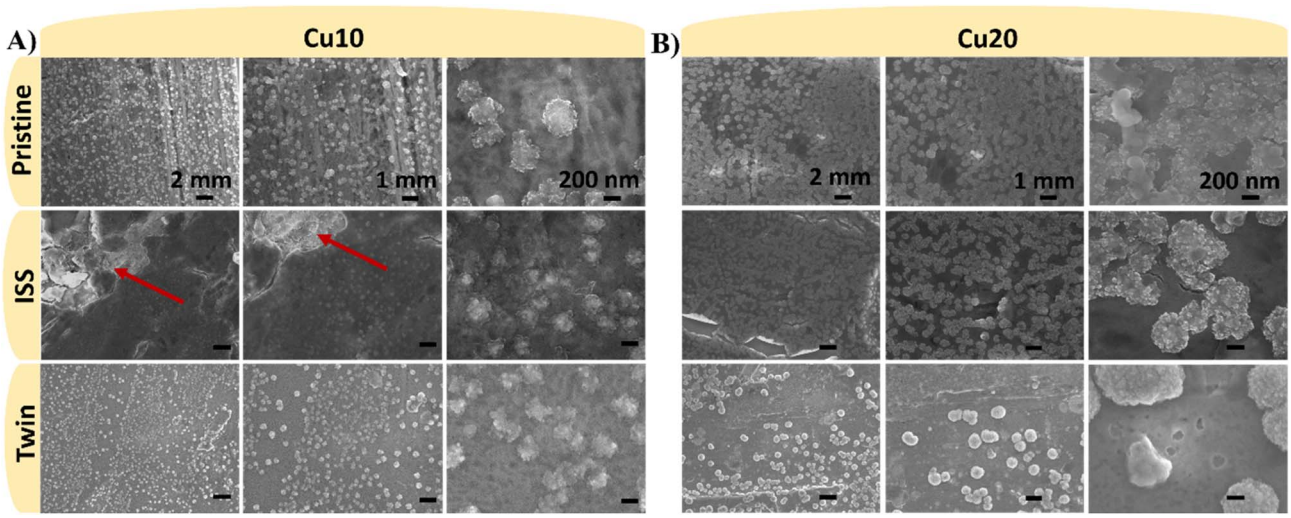


Fig. 2 Surface morphology of different coating samples on CRS in three different environmental conditions: as-coated, fresh samples (pristine), returned from the ISS after ~500 days exposure to the environment (ISS), and control twin. (A) Cu10, and (B) Cu20.

improved morphological stability of Cu20, the chemical nature of this protective behavior is examined in detail using XPS and XANES analysis in Sections 3.3 and 3.4.

The twin samples, stored under Earth ambient conditions, exhibit morphologies that closely resemble the pristine. Both Cu10 and Cu20 twin coatings show no signs of degradation, delamination, or surface evolution. The Cu clusters remain intact in size and distribution, confirming that the hybrid coatings are stable over time when not subjected to space-specific factors.

Overall, the SEM analysis demonstrates that while both Cu10 and Cu20 coatings offer substantial protection and morphological stability, Cu20 shows more resistance to space-induced surface degradation. The retention of large, intact Cu clusters under ISS conditions supports that a higher initial Cu concentration can enhance the environmental durability of the coating. These findings suggest the potential suitability of Cu–Zr hybrid coatings for long-term deployment in space, where oxidative conditions, temperature extremes, and material erosion are critical challenges.

### 3.2 Influence of Earth and outer space surrounding on the chemical dispersion of the coating

STEM-EDS mapping and elemental quantification were conducted to investigate how $Cu^{2+}$ concentration and environmental exposure influence the chemical distribution and Cu and Zr compositions in the hybrid CCs. Fig. 3 presents a comparative analysis between Cu10 and Cu20 coatings under pristine, ISS, and twin conditions, which reveal distinct trends in Cu localization, stability, and redistribution behavior. The coating depth for each sample condition was calculated using ImageJ and has been listed in Table S2.

In the Cu10 pristine sample Fig. 3A, the coating forms a uniform Zr-based matrix with finely dispersed nanoscale Cu clusters. These Cu-rich domains are embedded throughout the layer. Previous studies suggest that such clusters may exhibit a core–shell structure, with Cu embedded within a Zr-rich matrix.[12] The atomic ratio (%) profile for all the sample conditions is shown in Fig. 3B. The Cu : Zr atomic ratio profile is shown in Fig. 3C. The Cu : Zr atomic ratio for the pristine sample was 0.58 : 1, below the ~1 : 1 level reported in similar systems where larger Cu agglomerates can form, reducing coating uniformity and potentially compromising performance over time.[15] Upon exposure to the ISS environment, the Cu10 ISS sample shows pronounced Cu redistribution, with accumulation evident near both the coating surface and the coating–substrate interface. This redistribution is likely driven by a combination of harsh space-specific conditions. These conditions may influence the coating microstructure by facilitating the migration of metallic Cu species. In Zr–Cu conversion coatings, Cu is initially generated during the cathodic reduction step of the deposition process, wherein $Cu^{2+}$ ions gain electrons and are reduced to metallic Cu according to the reaction: $Cu^{2+} + 2e^- \rightarrow Cu$.[15] These Cu nanoparticles tend to coalesce through Ostwald ripening to minimize their surface energy, producing visible agglomerates[19] as highlighted in the white circle in Fig. 3A. In addition, atoms in the Cu nanoparticles are more mobile, thus promoting the migration and segregation of Cu toward energetically favorable regions, such as the metal–substrate interface, as highlighted in the yellow circle in Fig. 3A. The Cu : Zr atomic ratio is found to be 0.9 : 1 in the ISS sample, still below the literature level associated with extensive agglomeration.

Notably, a Si-rich layer is also observed at the outer surface of the Cu10 ISS sample, which is absent in pristine and twin conditions. This layer likely originates from the oxidation of volatile organosilicon species outgassed from spacecraft materials, which then condensed on sample surfaces and were converted to $SiO_2$ upon AO exposure. Silicone materials that have not been vacuum-baked often contain short-chain molecules that are volatile and can migrate onto nearby surfaces. When these contaminated surfaces are exposed to AO in LEO, the silicones oxidize to form silica.[20,21] During this process,

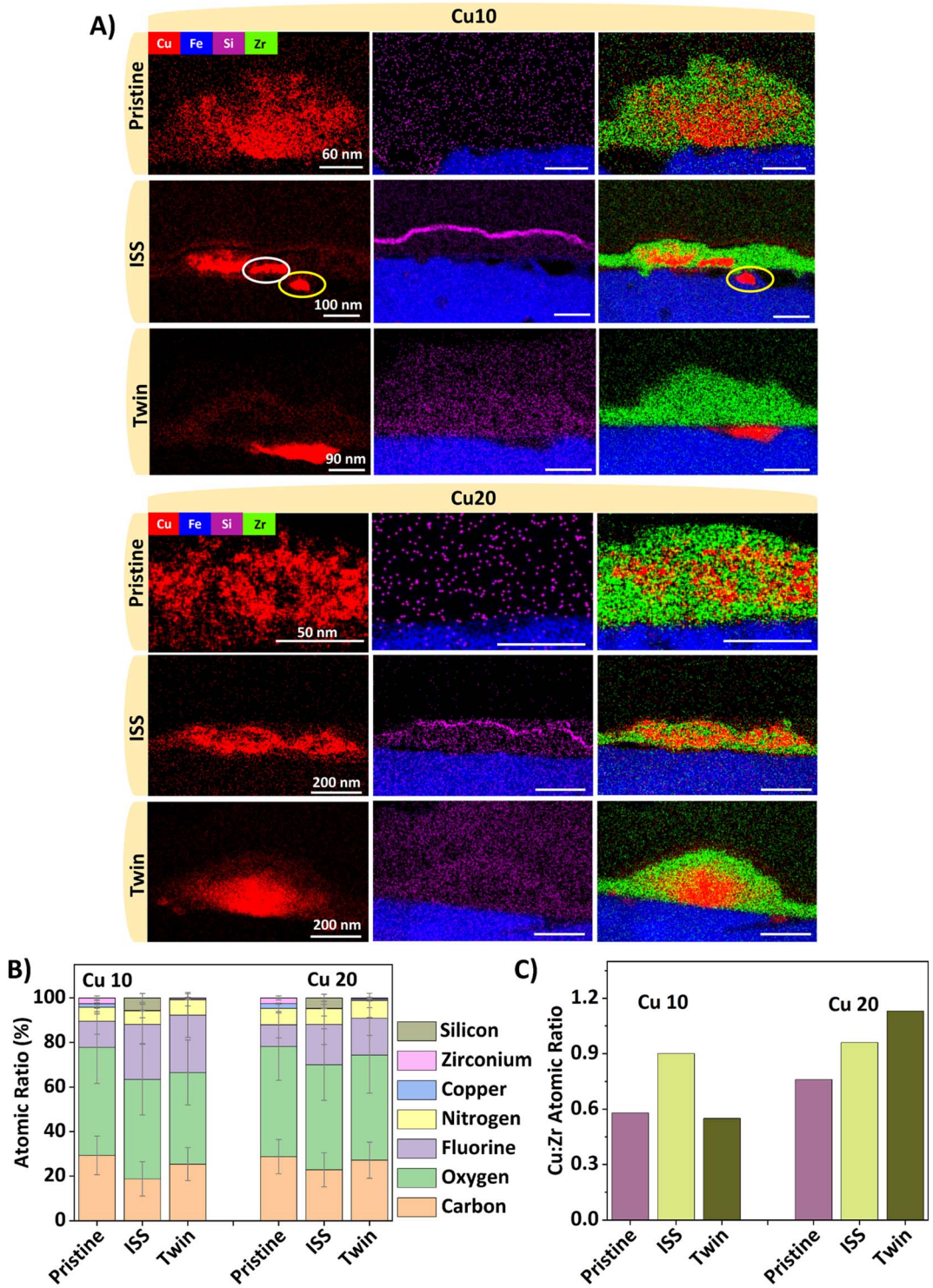


Fig. 3 STEM characterization of Cu10 and Cu20, highlighting their morphology and corresponding elemental distribution using EDS mapping. (A) Cu10 and Cu20; note the agglomeration of Cu indicated by the white circle and enrichment at the interface by yellow circle, (B) atomic ratio profile for all the sample conditions, and (C) Cu : Zr atomic ratio profile for all the sample conditions.

hydrocarbons can also become trapped on the surface. The resulting deposit forms an AO-protective layer, which can darken over time with continued solar radiation exposure.[18] In contrast, the Cu10 twin sample, stored at ambient conditions on Earth, shows only minor structural changes. A slight accumulation of Cu is observed near the interface, and the Cu : Zr ratio slightly decreases to 0.55 : 1. The Cu species migrates toward lower-energy interfacial regions *i.e.* the coating–substrate interface over time. Ambient storage produces some interfacial Cu enrichment, indicating that some redistribution

occurs even without LEO, likely due to aging/thermal cycling. Overall, the surface remains chemically stable in the absence of extreme environmental conditions.

To compare the effects of Cu20 *vs.* Cu10, the EDS mapping based on STEM analysis of the Cu20 samples is shown in Fig. 3C. The Cu20 pristine sample exhibits dense, well-defined Cu-rich domains embedded in the Zr-based matrix, consistent with its higher $Cu^{2+}$ concentration during the deposition process. The Cu : Zr ratio is 0.76 : 1, reflecting substantial Cu incorporation. After ISS exposure, the Cu20 ISS sample maintains a similar uniform distribution of Cu, no evident surface/interfacial accumulation, and the Cu : Zr ratio goes 0.96 : 1. Due to rapid oxidation under AO exposure, metallic Cu might form a $CuO/Cu_2O$ layer. These films are inherently less mobile due to strong Cu–O bonding and their semiconducting nature, effectively serving as a dense, passivating barrier that inhibits further diffusion and oxidation.[22] The immobilization of oxidized Cu results in no significant migration or accumulation toward the surface or interface. Because $Cu_2O$ and CuO have a larger molar volume than metallic Cu,[23] their formation during oxidation causes expansion, producing a oxide layer, restricting further Cu migration and preserving the overall uniform distribution. Additionally, a surface-bound $SiO_2$ layer is also present on the Cu20 ISS sample, likely formed *via* the same AO-driven oxidation of condensed siloxane species observed in Cu10. It seems to be uniformly distributed, forming an overlayer without interfering with the underlying Cu–Zr matrix. $SiO_2$ is widely recognized as an effective protective barrier against AO erosion in LEO due to its chemical inertness, high hardness, and resistance to further oxidation. This protective mechanism was shown in several studies and materials science analyses: the strong Si–O bonds in $SiO_2$ and already fully oxidized state render it highly resistant to the energetic AO flux found in LEO, so AO cannot further react with or erode the $SiO_2$ layer, unlike more reactive materials.[24] The $SiO_2$ surface film not only impedes further AO penetration but also remains adherent and continuous under harsh environmental conditions, preserving substrate integrity even after extended exposure. Additionally, experimental evidence shows that the formation and enrichment of $SiO_2$ on hybrid coatings leads to substantial reductions in mass loss and physical degradation under extreme AO fluence, confirming its function as a dense, passivating barrier.[25–27] Similar AO-induced silica layers have been documented in prior NASA exposure experiments, including MISSE and LDEF platforms.[27]

In the Cu20 twin sample, the Cu-rich domains are morphologically similar to those in the pristine sample. The Cu : Zr ratio increases to 1.13 : 1 for this sample. Interestingly, this ratio slightly exceeds the 1 : 1 threshold reported in literature, above which Cu agglomeration becomes more likely and can potentially compromise coating uniformity or long-term durability.[12] However, in this study, the coating remains morphologically intact, with no visible degradation or delamination, suggesting that the hybrid matrix can accommodate this level of Cu incorporation without adverse effects.

Taken together, these observations show that Cu10 coatings exhibit greater Cu mobility and agglomeration, resulting in localized Cu enrichment at the interface. In contrast, Cu20 coatings preserve a uniform dispersion of Cu species. Across all environmental conditions, the Zr-based matrix remains structurally intact and chemically stable, acting as a robust diffusion barrier that supports long-term environmental durability. These findings underscore the critical role of Cu concentration in dictating elemental redistribution and validate the potential of hybrid coatings for applications such as in space environments.

### 3.3 Analysis of chemical composition in surface coatings along the depth direction using XPS

XPS analysis provided detailed insights into how variations in Cu concentration and environmental exposure influence the chemical composition and oxidation behavior of the Cu–Zr hybrid coatings. The study focused on identifying the formation of Cu-containing species across the surface of Cu10 and Cu20 coatings under both Earth-stored and space-exposed conditions. These fitted Cu XPS spectra are presented in Fig. 4A and B respectively. The fitting parameters for Cu $2p_{3/2}$ XPS in Cu10 and Cu20 are shown in Table S1. The Cu $2p_{3/2}$ peak for both Cu10 and Cu20 is observed at 933.3 ± 0.1 eV, along with a shake-up satellite feature around ~942.0 eV, which is indicative of $Cu^{2+}$ in the form of copper(II) oxide (CuO).[28] In XPS, Cu(0) and Cu(I) cannot be reliably distinguished because their Cu $2p_{3/2}$ binding energies differ by less than 0.2 eV, and both lack the characteristic shake-up satellites as seen in Cu(II), and thus they are denoted as Cu(0)/Cu(I).

The atomic concentration (%) plot obtained for the Cu spectra using XPS for all the sample conditions is shown in Fig. S2. In the Cu10 pristine sample, the surface Cu exists in a mixed oxidation state, with a relatively higher fraction of Cu(0)/Cu(I) 37.23% compared to Cu(II), which is 31.06%. This is likely because of the cathodic deposition process during the formation of the conversion coating, during which $Cu^{2+}$ ions are electrochemically reduced to metallic Cu through the reaction: $Cu^{2+} + 2e^- \rightarrow Cu$, as reported previously.[29] Following deposition, some of these metallic Cu particles could undergo partial re-oxidation in the presence of dissolved oxygen or nitrate ($NO_3^-$) ions present in the coating solution or due to exposure to the environment over time. Recent studies[30,31] have particularly highlighted the role of nitrate ions in promoting the oxidation of Cu to $Cu_2O$ or CuO.

In the Cu10 twin sample the dominant Cu species is still Cu(0)/Cu(I) with 50.28%. The absence of significant shake-up satellite peaks for Cu(II) supports the dominance of Cu(0) or Cu(I), indicating that the surface remains largely chemically inert during Earth storage. After ISS exposure, the Cu10 ISS sample exhibits an increase in Cu(II) with 40.81% relative to Cu(0)/Cu(I), indicating enhanced oxidation of Cu under space conditions. These changes confirm that space-specific factors promote surface oxidation of Cu. In LEO, abundant UV radiation breaks apart $O_2$ molecules through photodissociation, producing AO by the following reactions:[32]

$$O_2 + \hbar\nu \rightarrow O + O \quad (1)$$

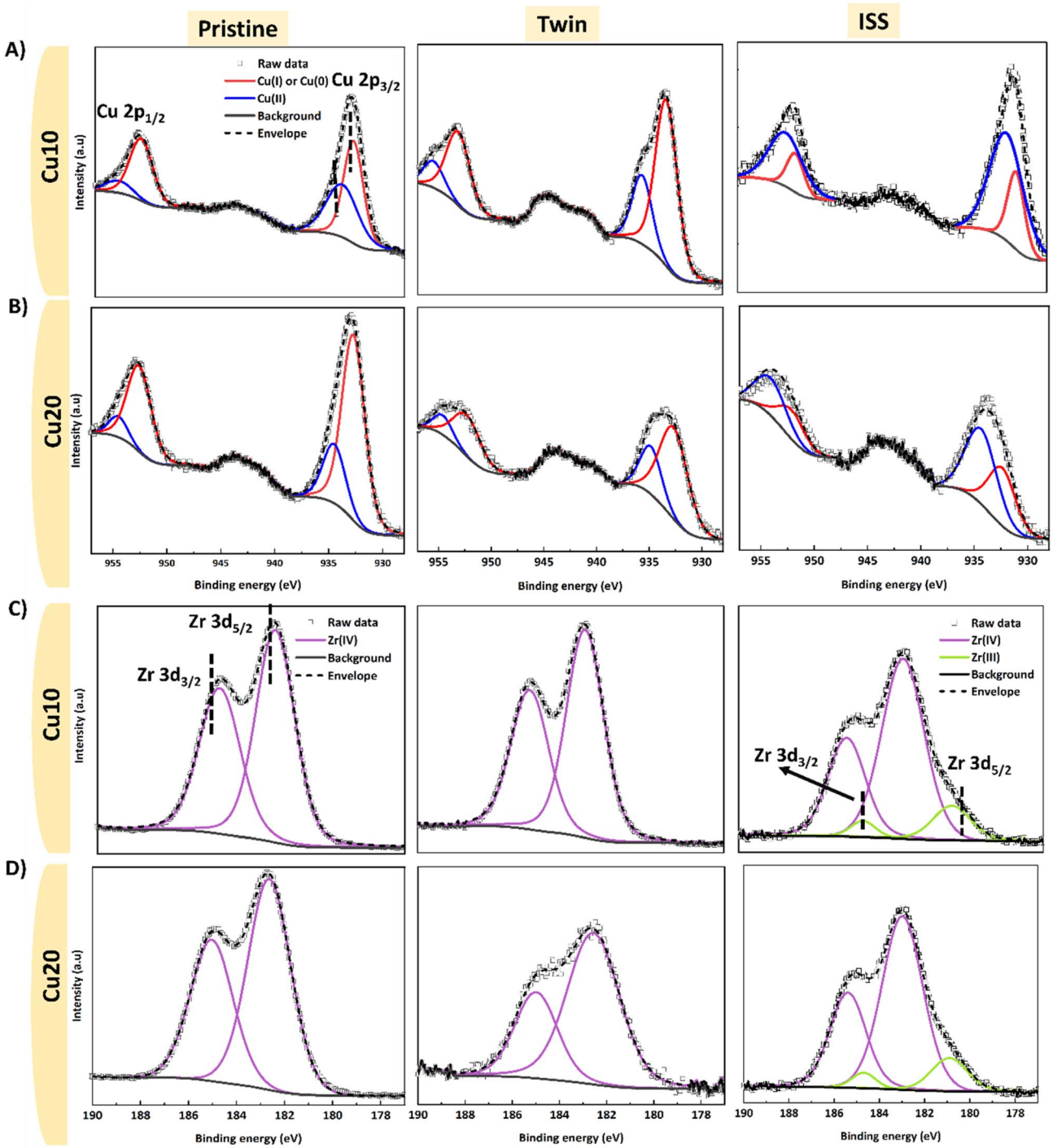


Fig. 4 Cu and Zr XPS spectra of coated samples. Cu spectra of (A) Cu10, (B) Cu20, Zr spectra of (C) Cu10 and, (D) Cu20.

or

$$O_2 + \hbar\nu \rightarrow O^+ + O \quad (2)$$

As a result, the atmosphere in LEO consists of approximately 96% AO. AO is highly reactive with metallic species such as Cu, Os, and Ag,[4] and readily interacts with exposed Cu surfaces. This reactivity accelerates oxidation processes, leading to the formation of CuO layers, as observed in the ISS-exposed Cu10 samples.[32]

The Cu20 pristine sample (Fig. 4B) shows a surface dominated by reduced Cu, with Cu(0)/Cu(I) accounting for 53.21%. The higher proportion of Cu(0)/Cu(I) in Cu20 in comparison to Cu10 pristine suggests that an increased initial $Cu^{2+}$ concentration in the solution promoted greater Cu incorporation into the coating. As a result, Cu20 shows a higher Cu in metallic or in reduced state compared to Cu10, reflecting the strong influence

of precursor concentration on the distribution of Cu within the hybrid coating. Cu20 twin Cu XPS spectra, also with a higher portion of Cu(0)/Cu(I). Upon exposure to the space environment, the Cu20 ISS sample undergoes a transformation Cu(II) becomes the dominant species at 49.05%, while Cu(0)/Cu(I) drops to 22.09%. As mentioned above, this oxidation is primarily driven by reactive AO in the LEO environment, which oxidizes surface Cu(0) and Cu(I) through sequential electron-loss steps. The higher Cu content in the Cu20 coating increases the amount of surface Cu atoms available for oxidation, making it susceptible to AO attack, explaining the more significant change compared to Cu10. This AO readily oxidizes surface Cu species through sequential reactions:[33]

$$2Cu + O \rightarrow Cu_2O \quad (3)$$

$$Cu_2O + O \rightarrow 2CuO \quad (4)$$

According to the literature, Cu is well known to form two common oxide phases – cuprous oxide ($Cu_2O$) and cupric oxide (CuO), depending on the surrounding oxidation conditions. $Cu_2O$ is the most stable and readily formed copper oxide under both low-oxygen and ambient conditions. In vacuum or low-pressure environments, limited oxygen availability restricts oxidation to $Cu_2O$, while in ambient air at room temperature, $Cu_2O$ still forms preferentially as the initial oxide due to its lower oxygen requirement and thermodynamic stability at moderate temperatures. Oxidation to CuO requires elevated temperatures or prolonged exposure. Also, CuO can readily reduce back to $Cu_2O$ when heated under vacuum.[34]

Given that our samples were exposed to the LEO environment, we can expect $Cu_2O$ to be the dominant oxidation product within the bulk of the coating. The vacuum conditions and limited ambient oxygen support $Cu_2O$ formation, while CuO may still form as a surface-localized phase due to the prolonged exposure to the AO, which can oxidize Cu and Cu(I). This is consistent with our XPS results, which reveal the presence of Cu(II) species and satellite features indicative of CuO. Since XPS is inherently surface-sensitive, typically probing only the top ~5–10 nm, the detected CuO is likely confined to the outermost surface layer. To confirm the bulk composition, XANES was conducted, which is further discussed in Section 3.3.

Fig. 4C and D show the fitted Zr XPS spectra respectively. In both Cu10 pristine and twin samples, the Zr 3d peaks are fully consistent with Zr(IV), confirming the presence of stable $ZrO_2$ under both as-deposited and Earth-stored conditions. In contrast, the Cu10 ISS sample still displays Zr(IV) as the main species but develops a shoulder near ~181 eV, indicative of partial reduction to Zr(III)[35] with an atomic concentration of 8.84%. This change is likely due to redox coupling with surface Cu, where AO-driven oxidation of $Cu^0$ to $Cu^{2+}$ releases electrons that reduce adjacent Zr(IV) sites. Prior studies confirm that $ZrO_2$ can accommodate such excess electrons through the Zr(IV) → Zr(III) transition.[36,37] The fitting parameters for Zr $3d_{3/2}$ XPS in ISS Cu10 and Cu20 are shown in Table S3.

The Cu20 pristine and Cu20 twin coatings both show strong Zr(IV) signals, with no evidence of the Zr(III), indicating that the $ZrO_2$ matrix remains chemically stable during deposition and subsequent Earth storage. In the Cu20 ISS sample, however, the spectra reveal Zr(IV) along with a clear shoulder at ~181 eV, confirming the presence of $Zr^{3+}$ with an atomic concentration of 10.94%. As with Cu10, this transformation arises from interfacial redox coupling: under AO exposure in space, Cu(0)/Cu(I) oxidize to Cu(II), as shown in eqn (3) and (4), releasing electrons that are subsequently captured by nearby Zr(IV) sites in the $ZrO_2$ lattice. The accepted electrons reduce Zr(IV) to Zr(III), as described by $Zr^{4+} + e^- \rightarrow Zr^{3+}$. When surface Cu(0)/Cu(I) is oxidized to Cu(II), electrons are transferred to oxygen species ($O \rightarrow O^{2-}$). At the Cu–$ZrO_2$ interface, however, not all the electron density remains on oxygen: the $ZrO_2$ matrix, like other reducible oxides, can accommodate excess charge by reducing lattice $Zr^{4+}$ to $Zr^{3+}$, thereby maintaining local charge-neutrality. Thus, the observed partial reduction of $Zr^{4+}$ to $Zr^{3+}$ in our ISS-exposed coatings reflects interfacial charge-transfer dynamics (*i.e.*, redox spillover) under AO-bombardment, rather than free electrons in isolation.[38]

The Cu20 coating exhibits more pronounced redox changes due to its higher initial Cu concentration in the solution, which results in a greater amount of Cu near the surface. These domains provide abundant reactive sites that are directly exposed to AO, making them more susceptible to oxidation from Cu(0)/Cu(I) to Cu(II). Consequently, Cu20 shows a stronger coupling between Cu oxidation and Zr reduction compared to Cu10, consistent with the more pronounced $Zr^{3+}$ signal and $Cu^{2+}$ enrichment observed in the ISS-exposed samples.

### 3.4 Analysis of Zr and Cu compounds formation after exposure to different environmental conditions using XANES

To assess the bulk (sub-surface) oxidation states, Cu and Zr K-edge XANES and linear-combination fitting (LCF) were performed for Cu10 and Cu20 under pristine, twin, and ISS conditions using references (Cu, $Cu_2O$, CuO for Cu; and $ZrO_2$ for Zr). The Cu K-edge XANES spectra of Cu10 (Fig. 5A) and its corresponding LCF are shown in Fig. 5B. For Cu10, the pristine bulk contains a mixture of Cu, $Cu_2O$, and CuO, indicating partial oxidation during/after deposition. After Earth storage (twin), the bulk shifts toward higher CuO content with loss of $Cu_2O$, consistent with continued oxidation in ambient air over time, and a reduction in metallic Cu compared to pristine, resulting in an overall increase in CuO content. After ISS exposure, the bulk shows increased $Cu_2O$ and decreased Cu relative to pristine, while CuO remains approximately unchanged, indicating that AO in LEO converts remaining metallic Cu to Cu(I) ($Cu_2O$) without significantly growing the CuO fraction in the bulk.

Cu20 follows the same qualitative trends (Fig. 5C and D). In the Cu20 pristine sample, XANES reveals a mixture of Cu, $Cu_2O$, and CuO, with CuO present as the major phase. XPS (Fig. 4B), however, showed a surface richer in Cu(0)/Cu(I), indicating limited oxidation at the outermost layer. This can be explained by the different probing depths of XANES and XPS, where XANES captures deeper regions of the sample while XPS reflects the more surface-sensitive composition, consistent with depth-

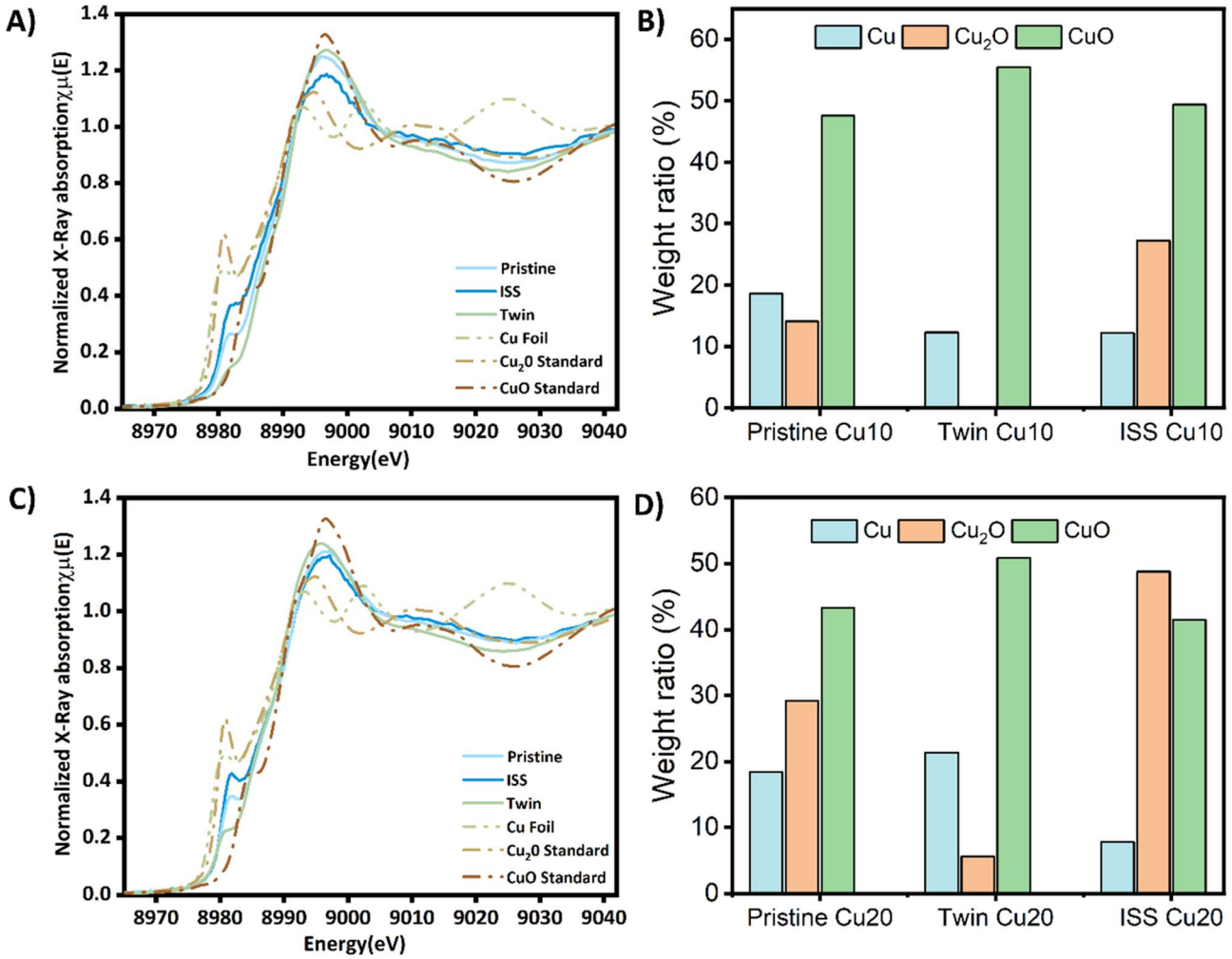


Fig. 5 XANES and LCF analysis of the samples at the Cu K-edge. (A) XANES of Cu10, (B) corresponding LCF of Cu10, (C) XANES of Cu20, and (D) corresponding LCF of Cu10.

dependent oxygen diffusion. Bulk CuO formed during deposition or early oxidation remains trapped due to the slow oxygen mobility at room temperature, while the surface continuously exchanges oxygen with the surrounding atmosphere and might re-equilibrates to the thermodynamically stable $Cu_2O$ phase. This depth-dependent redox profile, where $Cu_2O$-rich surface over CuO-rich bulk aligns with literature that surface CuO readily reverts to $Cu_2O$ under ambient conditions, while deeper oxides remain unchanged.[39] The Cu20 twin sample in Fig. 5D further supports this trend: the bulk is oxidized to CuO, consistent with sustained exposure to Earth's atmosphere during storage. In contrast, XPS in Fig. 4B still shows a surface with more concentration of Cu(0)/Cu(I), pointing to a depth-dependent oxidation gradient as stated above.

The most striking changes are observed in the Cu20 ISS sample. In Cu20 ISS, the bulk $Cu_2O$ fraction increases with a drop in Cu fraction, implying that metallic Cu is primarily oxidized to $Cu_2O$ under LEO exposure rather than to additional CuO. This indicates that AO exposure in LEO favors $Cu_2O$ formation over further conversion to CuO. The higher $Cu_2O$ content in the Cu20 ISS sample compared to Cu10 ISS is likely due to the greater availability of metallic Cu for oxidation, arising from the initially higher $Cu^{2+}$ concentration in the coating solution. XPS analysis of the Cu20 ISS sample confirmed the presence of more CuO at the surface, resulting in a layered structure, where CuO localized at the surface and $Cu_2O$ dominating the interior.

The Zr K-edge spectra of all samples, Cu10 and Cu20, as shown in Fig. S3 under all three conditions, match the $ZrO_2$ reference. This confirms that Zr remains in the fully oxidized 4+ state, Zr(IV), as $ZrO_2$ regardless of environmental exposure. The stability of Zr throughout all conditions further supports the role of the Zr-rich matrix as a chemically inert that preserves its structure under both Earth-based and space environments.

Overall, the XANES and LCF results show that the bulk of both Cu10 and Cu20 coatings contain mixed-valence Cu species, primarily in oxidized forms (CuO and $Cu_2O$), with their relative proportions varying under different exposure conditions. The bulk Zr component remains fully oxidized and chemically stable in all cases. These observations are consistent with the EDS-STEM data, together confirming that the Cu–Zr

hybrid CCs maintain chemical stability across diverse environments, supporting their potential for space applications.

### 3.5 Formation mechanism

To comprehensively understand the chemical and structural evolution of Cu–Zr hybrid conversion coatings, we propose a mechanistic pathway that accounts for coating synthesis, oxidation behavior, redox stratification, and environmental effects specific to Earth and LEO as shown in Fig. 6. During the initial deposition process, $H_2ZrF_6$ provides $Zr^{4+}$ ions, while $Cu^{2+}$ ions are co-introduced as additives. On immersion, $ZrF_6^{2-}$ undergoes hydrolysis, forming a zirconium oxide/hydroxide layer on the steel substrate:

$$ZrF_6^{2-} + 4OH^- \rightarrow ZrO_2 \cdot 2H_2O + 6F^- \quad (5)$$

Simultaneously, $Cu^{2+}$ ions are electrochemically reduced on the cathodic metal surface:

$$Cu^{2+} + 2e^- \rightarrow Cu \quad (6)$$

The reduced Cu nucleates as nanoclusters embedded within the $ZrO_2$ matrix, forming a chemically hybrid conversion coating. These clusters may adopt a core–shell morphology or remain as nanoscale inclusions, influenced by Cu concentration and reaction kinetics. Under Earth conditions (pristine and twin samples), the coating is exposed to atmospheric oxygen and moisture. Here, a stepwise oxidation of Cu occurs: firstly, metallic Cu oxidizes to cuprous oxide:

$$4Cu + O_2 \rightarrow 2Cu_2O \quad (7)$$

Secondly, $Cu_2O$ is further oxidized to CuO in the presence of sustained $O_2$ exposure:

$$2Cu_2O + O_2 \rightarrow 4CuO \quad (8)$$

This oxidation proceeds inward from the surface. In the pristine state, only partial oxidation occurs, reflected in a mixed state of Cu, Cu(I), and Cu(II) observed in both XANES and XPS. Over time, in the twin samples, oxygen diffusion into the bulk increases, oxidizing Cu more fully to CuO.

In contrast, space-exposed samples experience a different environment. In LEO, ultra-high vacuum, rapid thermal cycling, and AO flux give rise to a bifurcated behavior: in the bulk, CuO is reduced to $Cu_2O$. This is thermodynamically favorable in vacuum conditions where low oxygen partial pressure stabilizes $Cu^+$ over $Cu^{2+}$:[40]

$$4CuO \xrightarrow{\text{vacuum, } T} \uparrow 2Cu_2O + O_2 \quad (9)$$

Thermal cycling enhances atomic mobility, promoting thermally induced redox processes and diffusion across Cu-rich domains. XANES confirms increased $Cu_2O$ fractions and reduced CuO content in ISS samples compared to Earth-stored controls.

At the surface, AO bombardment leads to direct oxidation of exposed $Cu^0/Cu^+$ to $Cu^{2+}$:

$$2Cu + O \rightarrow Cu_2O \quad (10)$$

$$Cu_2O + O \rightarrow 2CuO \quad (11)$$

This process forms a thin, stable CuO-rich overlayer. XPS detects this surface enrichment, confirming AO interaction limited to the outer ~5–10 nm, whereas the underlying bulk characterized by XANES shows $Cu_2O$. Furthermore, a coupled redox mechanism between Cu and Zr is evident in ISS samples. As $Cu^0$ is oxidized at the surface, electrons are released and may migrate to nearby Zr(IV), reducing them to Zr(III).

Overall, in the ISS environment, the coatings develop a surface-passivating CuO layer, stable $Cu_2O$ in the bulk, and partial

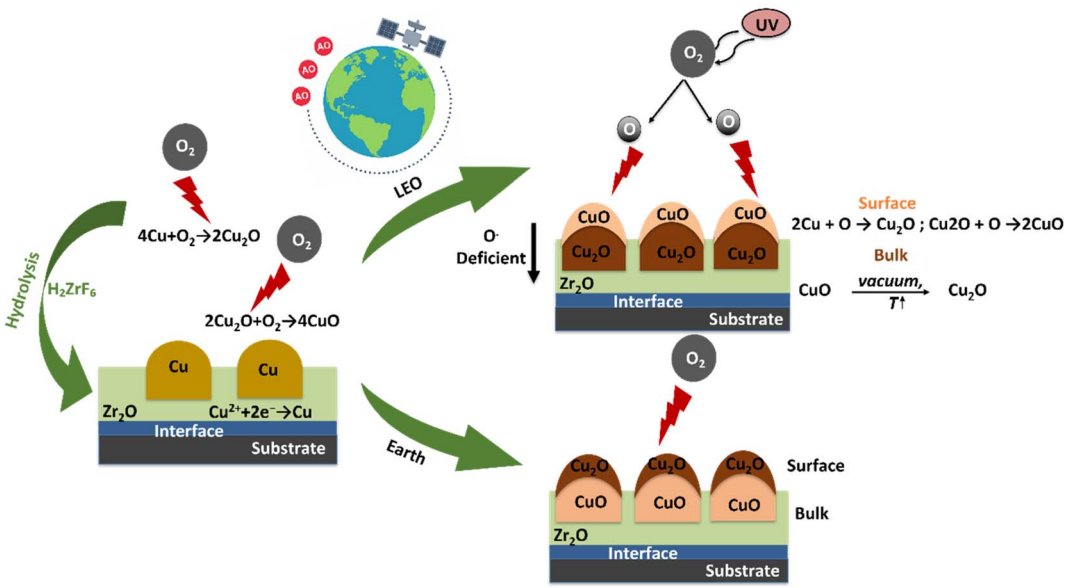


Fig. 6 Schematic illustration of the coating formation in the LEO and on Earth environment.

reduction of the Zr matrix, resulting in a layered, redox-active hybrid structure. By contrast, exposure on Earth drives continuous oxidation of the bulk toward CuO, while stabilizing $Cu_2O$ on the surface. This comparison highlights how different environments lead to distinct phase formations within the coatings.

### 3.6 Conclusion

This study systematically explored the chemical and morphological evolution of Cu-incorporated Zr-based hybrid CCCs deposited on cold-rolled steel, under both terrestrial and LEO environments. Using a multimodal characterization approach—comprising SEM, STEM-EDS, XANES, and XPS—we show that these coatings maintain their integrity under extreme space conditions, including atomic oxygen exposure and thermal cycling. While both Cu10 and Cu20 coatings exhibit robust performance, higher Cu content enhances resistance to space-induced surface degradation, indicating that Cu plays a key role in stabilizing the coating under oxidative environment. Across all conditions, the Zr matrix remained morphologically intact. Notably, a silicon-rich surface layer was detected exclusively in ISS-exposed samples, attributed to the AO-induced oxidation of volatile organosilicon species originating from spacecraft outgassing.

XANES and XPS analyses show that Cu in the coatings is predominantly oxidized, with Earth-stored samples gradually evolving toward CuO, while ISS-exposed samples develop a distinct depth-dependent redox structure characterized by CuO-enriched surfaces and $Cu_2O$-rich interiors. This stratified oxidation behavior, accompanied by interfacial Cu–Zr redox coupling, is unique to the space environment and reflects the combined effects of atomic oxygen exposure and vacuum conditions.

In conclusion, this study demonstrates that Zr-based hybrid chemical conversion coating (CCC) with Cu additives exhibit exceptional chemical resilience, structural integrity, and ability to adjust to harsh space conditions. The $ZrO_2$ matrix acts as a diffusion barrier and support, while Cu provides functional redox activity that buffers against oxygen-related damage. The LEO environment induces a beneficial stratified structure through surface oxidation and internal changes in electron gain and loss, sustaining the coating durability without compromising protection. These findings validate the potential of Cu–Zr hybrid coatings as sustainable, high-performance alternatives to chromate-based systems for aerospace and low-orbital applications, while also underscoring the importance of optimizing Cu content to tune redox behavior and surface response in multifunctional protective systems.

## Conflicts of interest

There are no conflicts to declare.

## Data availability

Part of the data supporting this article have been included as part of the supplementary information (SI). Supplementary information: Figure S1 MISEE 13 Certificate of the mission; Table S1 Fitting parameters for Cu $2p_{3/2}$ XPS in Cu10 and Cu20; Table S2 Coating depth for each sample condition; Figure S2 Atomic concentration obtained using XPS (%) for all the sample conditions for Cu species; Table S3 Fitting parameters for Zr $3d_{5/2}$ XPS in ISS Cu10 and Cu20; Figure S3 XANES of various samples for Zr K-edge. See DOI: https://doi.org/10.1039/d5ra09810f.

Full datasets from STEM, XPS, and XANES analyses is deposited in a public Zenodo repository; see DOI: https://doi.org/10.5281/zenodo.18854224.

## Acknowledgements

This work was funded by Henkel Corp. under award 81113. This research used resources and Beamline for Materials Measurement (BMM) of the National Synchrotron Light Source II, a U.S. Department of Energy (DOE) Office of Science User Facility operated for the DOE Office of Science by Brookhaven National Laboratory under Contract No. DE-SC0012704. The authors are grateful to Dr Bruce Ravel (National Institute of Standards and Technology), Lead Beamline Scientist at the BMM beamline, for his expertise and support on XAS characterization at BMM. This research used Electron Microscopy Facility and Proximal Probes Facility from the Center for Functional Nanomaterials, which is a U.S. DOE Office of Science Facility, at Brookhaven National Laboratory under Contract DESC0012704. The cost associated with sending samples to the ISS was supported by start-up funding from Stony Brook University provided to Prof. Chen-Wiegart.

## References

1 A. Grillo, *Low Earth Orbit (LEO): An Overview*, https://www.deepinsecurity.com/low-earth-orbit/.
2 M. M. Finckenor and K. K. de Groh, *Researchers Guide Space Environment Effects*, 2015.
3 M. M. Finckenor and K. K. de Groh, *Materials for Spacecraft*, 2018.
4 A. d. Rooij, *Corrosion in Space*.
5 M. M. Finckenor and C. George, *Marshall Analysis of International Space Station Vehicle Materials Exposed on Materials International Space Station Experiment from 2001 to 2011*, 2013.
6 K. Thirupathi, *The Study of Chromate Conversion Coating on Space Metallic Hardwares*, 2006.
7 H. John and D. Jeffrey, Chrome-Free Aluminum Coating System, *Materials* 8 Process Engineering, United Space Alliance, LLC, 2010.
8 A. M. Pereira, G. Pimenta and B. D. Dunn, *Assessment of Chemical Conversion Coatings for the Protection of Aluminium Alloys*, ESA Communication Production Office ESTEC, Noordwijk, The Netherlands, 2008.
9 H. R. Asemani, P. Ahmadi, A. A. Sarabi and H. E. Mohammadloo, Effect of zirconium conversion coating: adhesion and anti-corrosion properties of epoxy organic coating containing zinc aluminum polyphosphate

(ZAPP) pigment on carbon mild steel, *Prog. Org. Coat.*, 2016, **94**, 18–27.

10 X. Liu, D. Vonk, H. Jiang, K. Kisslinger, X. Tong, M. Ge, E. Nazaretski, B. Ravel, K. Foster, S. Petrash and Y.-C. K. Chen-Wiegart, Environmentally Friendly Zr-Based Conversion Nanocoatings for Corrosion Inhibition of Metal Surfaces Evaluated by Multimodal X-ray Analysis, *ACS Appl. Nano Mater.*, 2019, **2**(4), 1920–1929.

11 K. Kamburova, N. Boshkova, N. Boshkov and T. Radeva, Hybrid Zinc Coating with CuO Nanocontainers Containing Corrosion Inhibitor for Combined Protection of Mild Steel from Corrosion and Biofouling, *Coatings*, 2022, **12**(9), 16.

12 A. Mohanty, X. Y. Liu, C. C. Chung, D. Vonk, K. Kisslinger, X. Tong, A. Kiss, G. Halada, S. Petrash, K. Foster and Y. C. K. Chen-Wiegart, The effect of copper additives on hybrid Zr-based chemical conversion coating morphology and chemical compositions, *Appl. Surf. Sci. Adv.*, 2025, **27**(100726).

13 X. Y. Liu, D. Vonk, H. Jiang, K. Kisslinger, X. Tong, M. Y. Ge, E. Nazaretski, B. Ravel, K. Foster, S. Petrash and Y. C. K. Chen-Wiegart, Environmentally Friendly Zr-Based Conversion Nanocoatings for Corrosion Inhibition of Metal Surfaces Evaluated by Multimodal X-ray Analysis, *ACS Appl. Nano Mater.*, 2019, **2**(4), 1920–1929.

14 X. Y. Liu, D. Vonk, K. Kisslinger, X. Tong, G. Halada, S. Petrash, K. Foster and Y. C. K. Chen-Wiegart, Unraveling the Formation Mechanism of a Hybrid Zr-Based Chemical Conversion Coating with Organic and Copper Compounds for Corrosion Inhibition, *ACS Appl. Mater. Interfaces*, 2021, **13**(4), 5518–5528.

15 A. Mohanty, X. Liu, C.-C. Chung, D. Vonk, K. Kisslinger, X. Tong, A. Kiss, G. Halada, S. Petrash, K. Foster and Y.-c. K. Chen-Wiegart, The effect of copper additives on hybrid Zr-based chemical conversion coating morphology and chemical compositions, *Appl. Surf. Sci. Adv.*, 2025, **27**, 100726.

16 D. R. Vonk, I. T. S. Smith, A. Bobadilla, *Thin Corrosion Protective Coatings Incorporating Polyamidoamine Polymers*, 2021, MX2017013123A.

17 B. Ravel and M. Newville, ATHENA, ARTEMIS, HEPHAESTUS: data analysis for X-ray absorption spectroscopy using IFEFFIT, *J. Synchrotron Radiat.*, 2005, **12**(4), 537–541.

18 M. M. Finckenor and K. K. de Groh, *International Space Station (ISS) Researcher's Guide*, NASA, ISS Research Integration Office, 2015.

19 V. I. Pryakhina, B. I. Lisjikh, V. A. Lebedev, S. A. M. Tofail and V. Y. Shur, Temperature controlled morphology transformation during aging of colloidal copper nanoparticles produced by laser ablation in water, *Mater. Today Commun.*, 2023, **35**, 105939.

20 B. Banks, S. Miller, T. Stueber, A. Snyder, K. de Groh, C. Haytas and D. Brinker, *Issues and Effects of Atomic Oxygen Interactions with Silicone Contamination on Spacecraft in Low Earth Orbit*, Glenn Research Center, 2000.

21 T. Harty, Effects of Atomic Oxygen on the Vacuum-Induced Mass Loss Properties of a Variety of Spacecraft Materials, California Polytechnic State University, Masters Thesis, San Luis Obispo, 2017.

22 A. A. Samokhvalov, N. A. Viglin, B. A. Gizhevskii, N. N. Loshkareva, V. V. Osipov, N. I. Solin and Y. P. Sukhorukov, Low-mobility charge carriers in CuO, *J. Exp. Theor. Phys.*, 1993, **76**(3), 463–468.

23 G. Fritz-Popovski, F. Sosada-Ludwikowska, A. Köck, J. Keckes and G. A. Maier, Study of CuO Nanowire Growth on Different Copper Surfaces, *Sci. Rep.*, 2019, **9**, 807.

24 L. R. Schmidt, J. Francoeur, A. Aguero, M. R. Wertheimer, J. E. Klemberg-Sapieha, L. Martinu, J. W. Blezius and M. Olivier, *The Strategic Technologies for Automation and Robotics (Stear) Program Protection of Materials in the Space Environment Subprogram*.

25 S. Zhou, L. Zhang, L. Zou, B. I. Ayubi and Y. Wang, Mechanism Analysis and Potential Applications of Atomic Oxygen Erosion Protection for Kapton-Type Polyimide Based on Molecular Dynamics Simulations, *Polymers*, 2024, **16**(12), 1687.

26 H. Qi, Q. Shi, Y. Qian, Y. Li, J. Xu, C. Xu, Z. Zhang and X. Xie, The Atomic Oxygen Erosion Resistance Effect and Mechanism of the Perhydropolysilazane-Derived SiOx Coating Used on Polymeric Materials in Space Environment, *Polymers*, 2022, **14**(2), 322.

27 J. Dever, B. Banks, K. K. de Groh and S. Miller, *Degradation of Spacecraft Materials, NASA Glenn Research*, 2004.

28 S. Poulston, P. M. Parlett, P. Stone and M. Bowker, Surface oxidation and reduction of CuO and Cu2O studied using XPS and XAES, *Surf. Interface Anal.*, 1996, **24**(12), 811–820.

29 T. Lostak, S. Krebs, A. Maljusch, T. Gothe, M. Giza, M. Kimpel, J. Flock and S. Schulz, Formation and characterization of $Fe^{3+}$-/$Cu^{2+}$-modified zirconium oxide conversion layers on zinc alloy coated steel sheets, *Electrochim. Acta*, 2013, **112**, 14–23.

30 A. Sarfraz, R. Posner, M. M. Lange, K. Lill and A. Erbe, Role of Intermetallics and Copper in the Deposition of $ZrO_2$ Conversion Coatings on AA6014, *J. Electrochem. Soc.*, 2014, **161**(12), C509–C516.

31 J. Cerezo, I. Vandendael, R. Posner, J. H. W. de Wit, J. M. C. Mol and H. Terryn, The effect of surface pre-conditioning treatments on the local composition of Zr-based conversion coatings formed on aluminium alloys, *Appl. Surf. Sci.*, 2016, **366**, 339–347.

32 C. E. Vest, The effects of the space environment on spacecraft surfaces, *Johns Hopkins APL Tech. Dig.*, 1991, **12**(1), 46–54.

33 A. G. Gusakov, A. G. Voropayev, M. L. Zheludkevich, A. A. Vecher and S. A. Raspopov, Studies of the interaction of copper with atomic and molecular oxygen, *Phys. Chem. Chem. Phys.*, 1999, **1**(23), 5311–5314.

34 G. N. Ra, J. C. Gregory and L. C. Christ, The interaction of atomic oxygen with copper: An XPS, AES, XRD, optical transmission, and stylus profilometry study, *LDEF: 69 Months in Space. Part 3: Second Post-Retrieval Symposium*, NASA, Langley Research Center, 1993.

35 D. Diniasi, F. Golgovici, A. H. Marin, A. D. Negrea, M. Fulger and I. Demetrescu, Long-Term Corrosion Testing of Zy-4 in

a LiOH Solution under High Pressure and Temperature Conditions, *Materials*, 2021, **14**(16), 4586.

36 C. Gionco, M. C. Paganini, E. Giamello, R. Burgess, C. Di Valentin and G. Pacchioni, Paramagnetic Defects in Polycrystalline Zirconia: An EPR and DFT Study, *Chem. Mater.*, 2013, **25**(11), 2243–2253.

37 M. F. Bekheet, L. Schlicker, R. Popescu, W. Riedel, M. Grünbacher, S. Penner and A. Gurlo, A quantitative microscopic view on the gas-phase-dependent phase transformation from tetragonal to monoclinic ZrO2, *J. Am. Ceram. Soc.*, 2024, **107**(7), 5036–5050.

38 A. R. Puigdollers, P. Schlexer, S. Tosoni and G. Pacchioni, Increasing Oxide Reducibility: The Role of Metal/Oxide Interfaces in the Formation of Oxygen Vacancies, *ACS Catal.*, 2017, **7**(10), 6493–6513.

39 S. K. Matam, P. K. Sharma, E. H. Yu, C. Drivas, M. D. Khan, M. Wilding, N. Ramanan, D. Gianolio, M. A. Isaacs, S. Guan, P. R. Davies and C. R. A. Catlow, Operando X-ray absorption spectroscopic flow cell for electrochemical $CO_2$ reduction: new insight into the role of copper species, *Catal. Sci. Technol.*, 2025, **15**(4), 1070–1081.

40 L. De Los Santos Valladares, D. Hurtado Salinas, A. B. Dominguez, D. A. Najarro, S. I. Khondaker, T. Mitrelias, C. H. W. Barnes, J. A. Aguiar and Y. Majima, Crystallization and electrical resistivity of Cu2O and CuO obtained by thermal oxidation of Cu thin films on SiO2/Si substrates, *Thin Solid Films*, 2012, **520**(20), 6368–6374.